Electronic Supplementary Information

Local symmetry breaking in SnO_2 nanocrystals with cobalt doping and its effect on the optical properties

S. Roy[a], Amish G. Joshi[b], S. Chatterjee[c] and Anup K. Ghosh[*a]

[a]*Materials Research Laboratory, Department of Physics, Institute of Science, Banaras Hindu University, Varanasi – 221005, India.*

[b]*CSIR-National Physical Laboratory, Dr. K.S. Krishnan Marg, New Delhi – 110012, India.*

[c]*Department of Physics, Indian Institute of Technology (Banaras Hindu University), Varanasi – 221005, India.*

**Email: akghosh@bhu.ac.in*

SI-Raman: Tin (IV) oxide crystallizes in rutile tetragonal structure with point group D_{4h}^{14} and space group $P4_2/mnm$. Since, each unit cell of SnO_2 consists of two Sn atoms and four O atoms (Z = 2), there are total of 18 (= 3n, n being the number of atoms per unit cell) branches for the vibrational modes in the first Brillouin zone. On the basis of group theory, the irreducible representation for normal lattice vibrational modes at Γ(0,0,0) point of the Brillouin zone is [1]:

$$\Gamma = {}^1\Gamma_1^+(A_{1g}) + {}^1\Gamma_2^+(A_{2g}) + {}^1\Gamma_3^+(B_{1g}) + {}^1\Gamma_4^+(B_{2g}) + 4\,{}^2\Gamma_5^+(E_u) + 2\,{}^1\Gamma_1^-(A_{2u}) + 2\,{}^1\Gamma_4^-(B_{1u}) + 2\,{}^1\Gamma_5^-(E_g) \quad \text{(S1)}$$

Among these 18 normal modes, 15 are optic modes and three modes are acoustic. One singly degenerate A_{2u} and three doubly degenerate E_u modes constitutes the IR active modes, the Raman active modes are three singly degenerate modes A_{1g}, B_{1g}, B_{2g} and the doubly degenerate mode E_g. The modes, the singly degenerate A_{2g} and both singly degenerate B_{1u} are silent modes. The remaining – one singly degenerate A_{2u} and one doubly degenerate E_u modes are acoustic. The Raman active modes consist of the vibrations of O atoms with the Sn atoms at rest. The modes A_{1g}, B_{1g} and B_{2g} correspond to the vibrations in a plane perpendicular to the c-axis whereas the mode E_g corresponds to vibrations in the direction of c axis. Both A_{1g} and B_{2g} are related to the expansion and contraction of Sn-O bonds, where, B_{2g} is an asymmetric vibrational mode involving the contraction of all the six Sn-O bonds, of the Sn octahedron, coordinately at the same time, and for the symmetric vibrational mode A_{1g} two Sn-O bonds contract and the other four Sn-O bonds either contract or expand in opposite ways. The B_{1g} mode corresponds to the rotation of the whole octahedron of O atoms around the c axis and E_g mode corresponds to the translation motion of oxygen atoms in oxygen plane [2, 3]. Classically, only the Raman active modes A_{1g} (at ~ 638cm^{-1}), B_{2g} (at ~ 782 cm^{-1}), E_g (at ~ 476 cm^{-1}) and sometimes low intensity B_{1g} (at ~ 123cm^{-1}) are found in the Raman spectrum of bulk SnO_2 crystals under backscattering geometry owing to the selection rule of $\vec{q} = 0$, i.e., only the phonons near the Brillouin zone center of an infinite periodic crystal contribute to the Raman scattering of incident photons; where, $\vec{q}$ is the wave-vector of the phonons satisfying the scattering conditions:

$$\overrightarrow{k_0} - \overrightarrow{k'} = 2\pi\vec{\tau} - \vec{q}$$

$$E_0 - E' = \pm h\nu$$

where, photons of energy $E_0 = \frac{\hbar^2 k_0^2}{2m_p}$ and momentum $\hbar\overrightarrow{k_0}$ are incident on the sample, and are back-scattered with energy $E' = \frac{\hbar^2 k'^2}{2m_p}$ and momentum $\hbar\overrightarrow{k'}$; $\vec{q}$ is the wave-vector, and hν is the energy of the phonons, +/- sign refer to the creation or annihilation of phonons during the scattering process such that Stokes' Raman shift corresponds to the creation of phonons; and τ is a reciprocal lattice vector [3]. However, when $\vec{q} = 0$ selection rule breaks down such that the phonons around the zone centre also contributes to the Raman spectra of nanocrystals, there occurs a wave-number shift with asymmetric broadening of the Raman active modes A_{1g}, B_{2g} and E_g as compared to the bulk crystals, and in some cases, forbidden modes become Raman active along with inclusion of some surface activated modes, which are otherwise absent in their bulk counterpart. Except the inclusion of forbidden phonon modes in Raman spectra of the SnO_2 nanocrystals, phonon dynamics of the wave number shift and the asymmetric broadening of the bulk Raman modes in the nanocrystals are best governed by the phonon dispersion curves based on the phonon confinement model [4].

SI-FTIR: Fig. 17 (main article) shows the FTIR spectra of the present $Sn_{1-x}Co_xO_2$ nanocrystals and table S4 lists the observed bands. The most prominent band observed in the region of 460 – 650 cm^{-1} corresponds to various Sn – O vibrations [5] of SnO_2 crystal structure. The band at 1384 cm^{-1} is arising from some impurity present in KBr used for dispersion of $Sn_{1-x}Co_xO_2$ nanocrystals for recording the spectra, which is confirmed by the most intense band at 1384 cm^{-1} in the FTIR spectrum of the KBr used, as shown in the inset of fig. 17 (main article). The band at 2345 cm^{-1} is assigned to asymmetric stretching vibrations of CO_2 molecules. The broad absorption band at around 3405 cm^{-1} and the relatively less broad band at 1634 cm^{-1} are assigned respectively to the asymmetric stretching vibrations of hydroxyl (-OH) groups and bending vibrations of H-O-H groups of H_2O molecules adsorbed on the surface of the nanocrystals. Since, as the Co doping concentration increases, the size of nanocrystals decreases (as evident from XRD and TEM) and hence the surface effects emerge, the increase in strength of -OH vibrational band at around 3405 cm^{-1} with doping indicates more presence of hydroxyl species covering the surface of nanocrystals ensuring completion of bonds for surface oxygen [5]. The above-mentioned bands in the spectral range of 1384 cm^{-1} - 3405 cm^{-1} are also present in the FTIR spectra of the host KBr matrix (shown in inset of fig. 17) used for recording the spectra which suggests that these bands might be originating because of a combination of the adsorption of the corresponding molecules on the surface of the nanocrystals and their presence in the host KBr. It can be seen that with increase in Co doping concentration, the width as well as the wave number position of the bands remain constant, such that Co doping have no effect on these bands, asserting the above conclusion as well as the purity of $Sn_{1-x}Co_xO_2$ nanocrystals. The band at around 1100 cm^{-1} might be due to Sn-OH vibrations [6]. The absence of any Co – OH bonds in the spectrum is due to limitation of instrument which might be because of very low doping concentration of cobalt in $Sn_{1-x}Co_xO_2$ system. The presence of such hydroxyl species make the nanocrystals to be easily dispersed in polar solvents and the dispersions are also stable such that they can be used in many opto-electronic applications.

SI-UV-Visible:

Determination of optical band gap from Tauc's plot: The optical band gap (E_g) of the present $Sn_{1-x}Co_xO_2$ nanocrystals have been determined experimentally by Tauc's plot using eqn. (S2):

$$F(R)h\nu = B(h\nu - E_g)^n \ldots\ldots\ldots\ldots\ldots\ldots\ldots\ldots\ldots (S2)$$

where, F(R) is the Kubelka-Munk function as described in eqn. (S3) and is proportional to the absorption coefficient (α):

$$F(R) = \frac{(1-R)^2}{2R} \ldots\ldots\ldots\ldots\ldots\ldots\ldots\ldots\ldots (S3)$$

hν is the incident photon energy, B is a constant and n = $\frac{1}{2}$, $\frac{3}{2}$, 2 or 3 depending upon the nature of electronic transition responsible for the absorption. For the determination of the optical band gap (E_g), $(F(R)h\nu)^{1/n}$ from eqn. (S2) is plotted as ordinate against the photon energy hν (in eV) as abscissa and the most linear region of the obtained curve is extrapolated to F(R) = 0. The point where the extrapolated line cuts the *x*-axis corresponding to F(R) = 0 yields the optical band gap of the semiconductor.

Determination of Urbach's energy: The Urbach type absorption is represented by:

$$\alpha(E) = \alpha_0 \exp\left(\frac{E}{E_u}\right) \ldots\ldots\ldots\ldots\ldots\ldots\ldots\ldots (S4)$$

where, α(E) is the absorption coefficient of the material at incident photon energy E, α_0 is a coefficient which depends upon the material and E_u is the Urbach energy. Since, F(R), given by eqn. (S3), is proportional to α(E), eqn. (S4) has been modified to eqn. (S5) for the determination of the Urbach energy of the present $Sn_{1-x}Co_xO_2$ nanoparticles:

$$F(R) = \alpha_0 \exp\left(\frac{E}{E_u}\right) \ldots\ldots\ldots\ldots\ldots\ldots\ldots\ldots (S5)$$

Hence,

$$\ln\big(F(R)\big) = \ln(\alpha_0) + \frac{E}{E_u} \ldots\ldots\ldots\ldots\ldots\ldots \quad (S6)$$

ln (F(R)) has been plotted as ordinate against the incident photon energy E as abscissa and the inverse of the slope of the linear fitting of the most linear portion of the graph directly gives the Urbach energy E_u of the semiconductors.

References:

1. A. Diéguez, A. Romano-Rodríguez, A. Vilá and J. R. Morante, *Journal of Applied Physics*, 2001, **90**, 1550–1557.
2. P. Sangeetha, V. Sasirekha and V. Ramakrishnan, *Journal of Raman Spectroscopy*, 2011, **42**, 1634–1639.
3. J. G. Traylor, H. G. Smith, R. M. Nicklow and M. K. Wilkinson, *Phys. Rev. B*, 1971, **3**, 3457–3472.
4. K. Roodenko, I. A. Goldthorpe, P. C. McIntyre and Y. J. Chabal, *Phys. Rev. B*, 2010, **82**, 115210.
5. L. Abello, B. Bochu, A. Gaskov, S. Koudryavtseva, G. Lucazeauand M. Roumyantseva, *Journal of Solid State Chemistry*, 1998, **135**, 78 – 85.
6. J. Suffner, P. Ágoston, J. Kling and H. Hahn, *Journal of Nanoparticle Research*, 2010, **12**, 2579–2588.

Table S1: Results from the Sn3d, O1s and Co2p core level X-ray photoemission spectroscopy (XPS) of the $Sn_{1-x}Co_xO_2$ (x = 0.00, 0.02 and 0.04) nanocrystals.

Co doping conc. (x)	*Cons-tituents*	*B.E. of XPS peak (in eV)*	*Origin of XPS peak*	*Spin-Orbit Splitting (in eV)*	*Oxidation state of constituent*	*FWHM of XPS peak (in eV)*	*Normalised Area (= Atomic Area/ASF)*	*Atomic % of Co constituents*			*Atomic Ratio of constituents*		
								Co_3O_4	Co^{2+}	Co^{3+}	Adsorbed O: Lattice O	Sn_i: Sn	δ
0.000	Sn	Sn 3d Core								-	0.37713	0	0.60223
		486.611	Lattice Sn $3d_{5/2}$ in SnO_2	8.41	+4	1.3	8739.642						
		495.021	Lattice Sn $3d_{3/2}$ in SnO_2										
	O	O 1s core											
		530.441	O^{2-} in SnO_2 lattice	-	-2	1.207	12216.043						
		531.579	Surface dangling bonds	-	-	1.956	4606.979						
0.020	Sn	Sn 3d Core									0.18683	0.06632	0.49301
		486.236	Lattice Sn $3d_{5/2}$ in SnO_2	8.41	+4	1.8	68198.739						
		494.646	Lattice Sn $3d_{3/2}$ in SnO_2										
		484.098	$3d_{5/2}$ of Sn_i	-	0	1.83	4522.777						
		477.859	Mg-$K_{\alpha 3}$ X-ray satellite peak w.r.t SnO_2 $3d_{5/2}$			1.74							
		476.066	Mg-$K_{\alpha 4}$ X-ray satellite peak w.r.t SnO_2 $3d_{5/2}$			1.77							
		O1s Core											

	O	529.816	O^{2-} in SnO_2 lattice	-	-2	1.7	116586.029						
		531.524	Surface dangling bonds	-		1.7	21782.325						
		519.772	Mg-$K_{\alpha 4}$ X-ray satellite peak w.r.t lattice O^{2-} in SnO_2	-		1.7							
		521.462	Mg-$K_{\alpha 3}$ X-ray satellite peak w.r.t lattice O^{2-} in SnO_2	-		1.7							
								14.8% of the total Co conc.	66.78 % of the total doped Co conc.	33.16 % Of the total doped Co conc.			
	Co	Co 2p Core											
		798.549	Doped Co^{2+} $2p_{1/2}$ principal peak	18.605	+2	3.43	2850.987						
		779.944	Doped Co^{2+} $2p_{3/2}$ principal peak			3.43							
		794.749	Doped Co^{3+} $2p_{1/2}$ principal peak	18.276	+3	3.43	1416.018						
		776.473	Doped Co^{3+} $2p_{3/2}$ principal peak			3.43							
		806.047	Doped Co^{2+} $2p_{1/2}$ satellite peak	22.422	+2	2.453	647.550						
		783.625	Doped Co^{2+} $2p_{3/2}$ satellite peak			3.638							
		795.808	Doped-precipitated out Co_3O_4 $2p_{1/2}$ principal peak	-		2	854.938						

		800.859	combination of x-ray energy loss of doped Co $2p_{3/2}$ and satellite of Co_3O_4			4.914							
		791.948	X-ray satellite corresponding to doped Co $2p_{1/2}$ state			3.364							
		773.298	X-ray satellite corresponding to doped Co $2p_{3/2}$ state			2.6							
0.040	Sn	Sn 3d Core						25.67% of the total Co conc.	43.99% of the total doped Co conc.	56% Of the total doped Co conc	0.20232	0.07201	0.34820
		486.588	Lattice Sn $3d_{5/2}$ in SnO_2	8.41	+4	1.81	55583.824						
		494.998	Lattice Sn $3d_{3/2}$ in SnO_2										
		484.527	$3d_{5/2}$ of Sn_i			1.6	4002.329						
		478.108	Mg-$K_{\alpha 3}$ X-ray satellite peak w.r.t SnO_2 $3d_{5/2}$			1.8							
		476.329	Mg-$K_{\alpha 4}$ X-ray satellite peak w.r.t SnO_2 $3d_{5/2}$			1.5							
	O	O 1s Core											
		529.925	O^{2-} in SnO_2 lattice	-	-2	1.7	102525.176						
		531.625	Surface dangling bonds	-		1.7	20742.954						
		520.021	Mg-$K_{\alpha 4}$ X-ray satellite			1.7							

			peak w.r.t lattice O^{2-} in SnO_2										
		521.636	Mg-$K_{\alpha 3}$ X-ray satellite peak w.r.t lattice O^{2-} in SnO_2			1.7							
	Co	Co 2p Core											
		799.438	Doped Co^{2+} $2p_{1/2}$ principal peak	18.95	+2	3.51	1935.133						
		780.488	Doped Co^{2+} $2p_{3/2}$ principal peak			3.509							
		798.288	Doped Co^{3+} $2p_{1/2}$ principal peak	18.08	18.605 +3	3.51	2462.973						
		780.208	Doped Co^{3+} $2p_{3/2}$ principal peak			3.51							
		805.776	Doped Co^{2+} $2p_{1/2}$ satellite peak	-	20.811 +2	3.145	1532.232						
		784.965	Doped Co^{2+} $2p_{3/2}$ satellite peak			4.464							
		795.735	Doped-precipitated out Co_3O_4 $2p_{1/2}$ principal peak	-		2.1	2048.912						
		801.825	combination of x-ray energy loss of doped Co $2p_{3/2}$ and satellite of Co_3O_4			3.459							

		792.625	X-ray satellite corresponding to doped Co $2p_{1/2}$ state			4.18							
		776.525	X-ray satellite corresponding to doped Co $2p_{3/2}$ state			2.638							

Table S2: Rietveld refinement parameters and important results of the $Sn_{1-x}Co_xO_2$ nanocrystals.

Doping Concentration (x)/ Constituents		Wyckoff Parameters		Normalised (w.r.t. 1) Site Occupancy	Bond Lengths (in nm)	Average Crystallite Size (in nm)	Lattice Parameters		d_{hkl} (in nm)	χ^2
		Wyckoff Site	Wyckoff Positions (x, y, z)				a = b (in nm)	c (in nm)		
x = 0.000 ($Co_{0.0}$)	Sn^{4+}	2a	x = 0.00000 y = 0.00000 z = 0.00000	0.986	d^{axial}_{O-Sn} = 0.20062 $d^{equatorial}_{O-Sn}$ = 0.20846	D_{S-S} = 11.42125 From TEM = 11.01nm	From Rietveld = 0.47381 (σ = 2.03973E-4)	From Rietveld = 0.31868 (σ = 9.43679E-6)	d_{110} = 0.33503 d_{101} = 0.26443	4.16
	O^{2-}	4f	x = 0.29809 y = 0.29809 z = 0.00000	0.903						
x = 0.005 ($Co_{0.5}$)	Sn^{4+}	2a	x = 0.00000 y = 0.00000 z = 0.00000	0.995	d^{axial}_{O-Sn} = 0.20116 $d^{equatorial}_{O-Sn}$ = 0.20888	D_{S-S} = 9.12197	From Rietveld = 0.47387 (σ = 2.03973E-4)	From Rietveld = 0.31871 (σ = 9.43679E-6)	d_{110} = 0.33507 d_{101} = 0.26446	4.05
	Co^{2+}	2a	x = 0.00000 y = 0.00000 z = 0.00000	0.0049						
	O^{2-}	4f	x = 0.29444 y = 0.29444 z = 0.00000	0.912						
x = 0.020 ($Co_{2.0}$)	Sn^{4+}	2a	x = 0.00000 y = 0.00000 z = 0.00000	0.972	d^{axial}_{O-Sn} = 0.19599 $d^{equatorial}_{O-Sn}$ = 0.2114	D_{S-S} = 8.2434	From Rietveld = 0.47364 (σ = 2.03973E-4)	From Rietveld = 0.31869 (σ = 9.43679E-6)	d_{110} = 0.33491 d_{101} = 0.26440	4.02
	Co^{2+}	2a	x = 0.00000 y = 0.00000 z = 0.00000	0.028						
	O^{2-}	4f	x = 0.29874 y = 0.29874 z = 0.00000	0.936						
x = 0.030 ($Co_{3.0}$)	Sn^{4+}	2a	x = 0.00000 y = 0.00000 z = 0.00000	0.969	d^{axial}_{O-Sn} = 0.18142 $d^{equatorial}_{O-Sn}$ = 0.21043	D_{S-S} = 7.71157 From TEM = 7.58 nm	From Rietveld = 0.47372 (σ = 2.03973E-4)	From Rietveld = 0.31870 (σ = 9.43679E-6)	d_{110} = 0.33497 d_{101} = 0.26442	3.87
	Co^{2+}	2a	x = 0.00000 y = 0.00000 z = 0.00000	0.030						
	O^{2-}	4f	x = 0.29866 y = 0.29866 z = 0.00000	0.949						

x = 0.040 ($Co_{4.0}$)	Sn^{4+}	2a	x = 0.00000 y = 0.00000 z = 0.00000	0.959	d_{O-Sn}^{axial} = 0.19266 $d_{O-Sn}^{equatorial}$ = 0.21347	D_{S-S} = 7.34007	From Rietveld = 0.47335 (σ = 2.03973E -4)	From Rietveld = 0.31870 (σ = 9.43679E -6)	d_{110} = 0.33470 d_{101} = 0.26436	3.90
	Co^{2+}	2a	x = 0.00000 y = 0.00000 z = 0.00000	0.040						
	O^{2-}	4f	x = 0.30201 y = 0.30201 z = 0.00000	0.986						

Table S3: Observed modes in Raman spectra of the $Sn_{1-x}Co_xO_2$ nanocrystals.

S/No.	Mode Identification as in fig. 10	Raman Shift (in cm^{-1})	Mode Description
01.	A_{1g}	633.32 – 631.84 (red shift)	A classical first order Raman mode ($^1\Gamma_1^+$)
02.	B_{1g}	188.28 – 182.16 (red shift)	A classical first order Raman mode ($^1\Gamma_3^+$)
03.	B_{2g}	776.59 – 758.96 (red shift)	A classical first order Raman mode ($^1\Gamma_4^+$)
04.	E_g	452.52 – 460.09 (blue shift)	A classical first order Raman mode ($^2\Gamma_5^-$)
05.	S1	249.59 – 243.60 (red shift)	A Disorder Activated Raman Mode ($^2\Gamma_5^+$(1) TO)
06.	S2	267.33 – 260.89 (red shift)	A Disorder Activated Raman Mode ($^2\Gamma_5^+$(1) LO)
07.	S3	316.87 – 299.68 (red shift)	A Disorder Activated Raman Mode ($^2\Gamma_5^+$(2) TO)
08.	S4	332.95 – 317.55 (red shift)	A Disorder Activated Raman Mode ($^2\Gamma_5^+$(2) LO)
09.	S5	359.29 – 355.90 (red shift)	A Second Order Raman Mode corresponding to classical first order Raman mode $^1\Gamma_3^+$
10.	S6	606.27 – 603.10 (red shift)	A Disorder Activated Raman Mode ($^2\Gamma_5^+$(3) TO)
11.	S7	715.07 – 723.19 (blue shift)	A Disorder Activated Raman Mode ($^1\Gamma_1^-$ LO)

Table S4: Observed Bands in the FTIR spectra of the $Sn_{1-x}Co_xO_2$ nanocrystals.

S/No.	Wave number (in cm^{-1})	Band Description
01.	627.62 – 620.16 (red shift)	Classically IR active TO $^2\Gamma_5^+$(3) (E_u(3)) mode (SnO asymmetric stretching vibrations in (xy0)-plane)
02.	480.96 – 474.74 (red shift)	Classically IR active TO $^1\Gamma_1^-$ (A_{2u}) mode (SnO asymmetric stretching vibrations along z-axis)
03.	529.95 – 522.16 (red shift)	Disorder activated IR $^1\Gamma_4^-$(2) (B_{1u}(2)) mode (Atomic displacements along z axis)
04.	≈ 1100 cm^{-1}	Sn-OH asymmetric stretching vibrations
05.	≈ 1384 cm^{-1}	Impurities in host KBr
06.	≈ 1634 cm^{-1}	Bending vibrations of surface adsorbed H-O-H group
07.	≈ 2345 cm^{-1}	Asymmetric stretching vibrations of surface adsorbed CO_2 molecules
08.	≈ 3405 cm^{-1}	Asymmetric stretching vibrations of surface adsorbed hydroxyl (-OH) group

Table S5: Band Gap, Hump energy and Urbach energy of the $Sn_{1-x}Co_xO_2$ nanocrystals.

Co Doping Concentration (x)	Band Gap (E_g^{alw}) (in eV)	Band Gap (E_g^{for}) (in eV)	Urbach Energy (E_u) (in eV)
0.000	3.69121	3.09632	0.25562
0.005	3.56065	2.8611	0.34344
0.020	3.53165	2.67604	0.39414

0.030	3.448	2.60699	0.44367
0.040	3.34309	2.46115	0.46242

Table S6: Room temperature PL peaks of the $Sn_{1-x}Co_xO_2$ nanocrystals along with their possible origin.

Co Doping Concentration (x)	**Peak Designation**	**Peak Wavelength**	**Region of EM Spectrum**	**Possible origin of Peak**
		(in nm)		
0	1	372.645	UV	eA^0transition
	2	381.845		eA^0-LO
	3	423.542	Visible (Violet)	V_O^x to A^0 transition
	4	435.201		
	5	446.188		
	6	460.313	Visible (Blue)	CBM to $V_O^{\bullet}$ And CBM to E_s
	7	486.771		
	8	496.860	Visible (Green)	Shallow trap states (V_O^x) to E_s
	9	508.520		
	10	519.730		
	11	529.820		
0.005	1	373.359	UV	eA_0 transition
	2	381.929		eA^0-LO
	3	422.118	Visible (Violet)	V_O^x to A_0 transition
	4	428.102		
	5	441.179		
	6	462.012	Visible (Blue)	CBM to $V_O^{\bullet}$ And CBM to E_s
	7	486.835		
	8	494.813	Visible (Green)	Shallow trap states (V_O^x) to E_s
	9	506.560		
	10	518.085		
	11	529.388		
	12	390.501	UV	eA^0-2LO
0.02	1	370.866	UV	eA_0 transition
	2	382.098		eA^0-LO
	3	422.484	Visible (Violet)	V_O^x to A_0 transition
	4	430.139		
	5	442.388		
	6	459.667	Visible (Blue)	CBM to $V_O^{\bullet}$ And CBM to E_s
	7	487.007		
	8	499.037	Visible (Green)	Shallow trap states (V_O^x) to E_s
	9	510.629		
	10	520.909		
	11	530.314		
	12	393.332	UV	eA^0-2LO

0.03	1	371.808	UV	eA_0 transition
	2	382.148		eA^0-LO
	3	423.670	Visible (Violet)	V_O^x to A_0 transition
	4	431.205		
	5	444.503		
	6	461.569	Visible (Blue)	CBM to $V_O^{\bullet}$ And CBM to E_s
	7	486.170		
	8	495.478	Visible (Green)	Shallow trap states (V_O^x) to E_s
	9	507.003		
	10	518.306		
	11	529.388		
	12	392.612	UV	eA^0-2LO
0.04	1	373.138	UV	eA_0 transition
	2	382.183		eA^0-LO
	3	422.783	Visible (Violet)	V_O^x to A_0 transition
	4	430.319		
	5	443.173		
	6	461.569	Visible (Blue)	CBM to $V_O^{\bullet}$ And CBM to E_s
	7	485.726		
	8	493.484	Visible (Green)	Shallow trap states (V_O^x) to E_s
	9	505.008		
	10	515.425		
	11	529.388		
	12	391.604	UV	eA^0-2LO
	13	520.079	Visible	

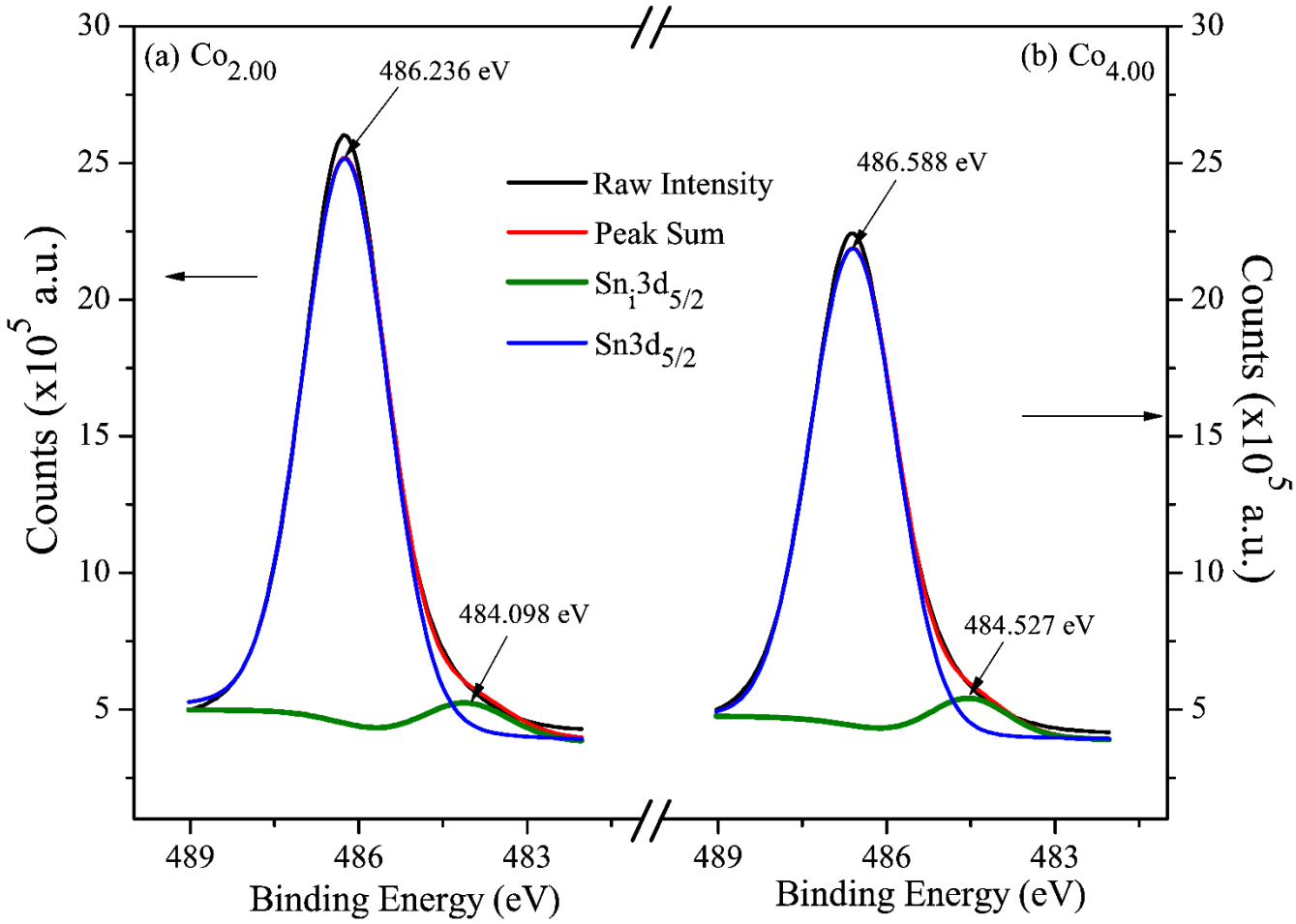

Fig. S1: Deconvoluted spectra of $Sn3d_{5/2}$ for $Co_{2.00}$ (x = 0.02) and $Co_{4.00}$ (x = 0.04) nanocrystals.

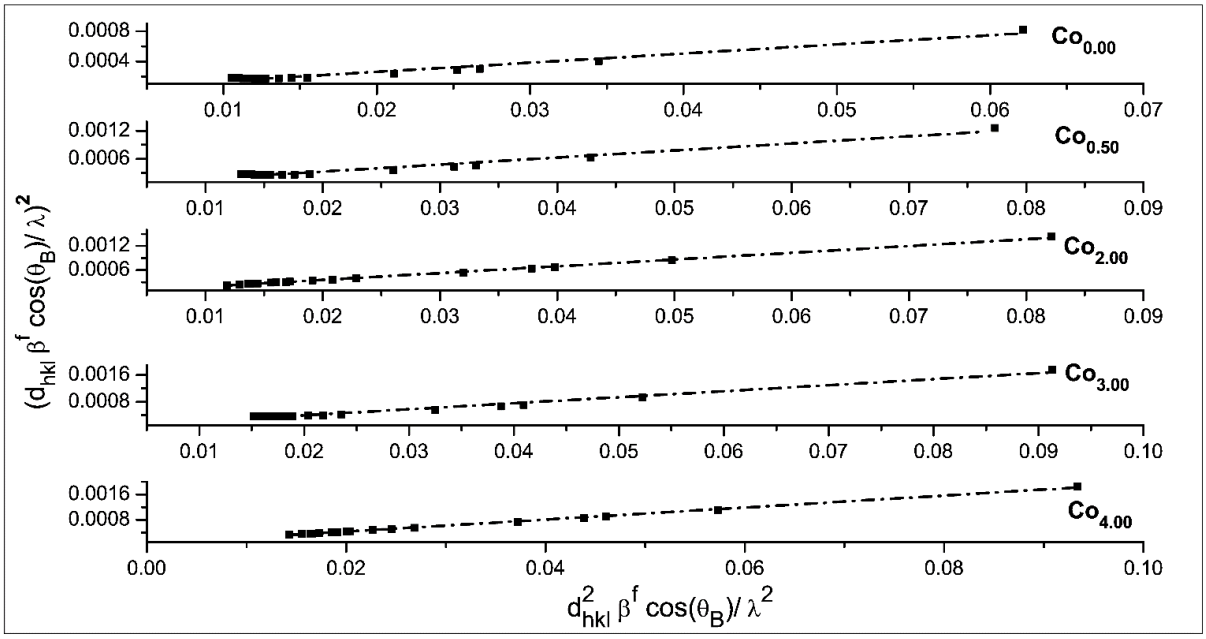

Fig. S2: Size-strain plots of the $Sn_{1-x}Co_xO_2$ nanocrystals to estimate the average crystallite size D_{S-S} and average lattice strain ε_{S-S}.

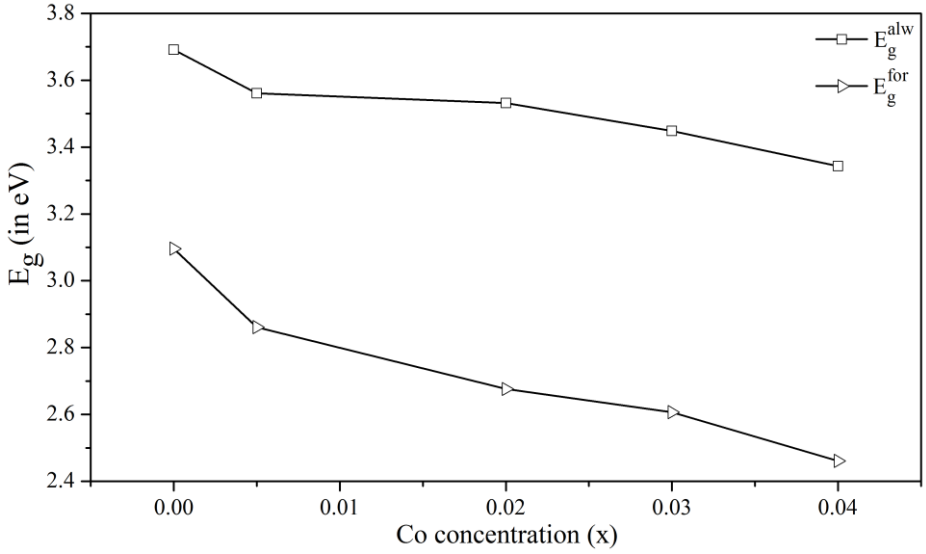

Fig. S3: Variation of direct allowed (E_g^{alw}) and direct forbidden (E_g^{for}) energy gaps of the $Sn_{1-x}Co_xO_2$ nanocrystals with Co doping concentration.